Biomedical Optics EXPRESS

Influence of probe pressure on the diffuse correlation spectroscopy blood flow signal: extra-cerebral contributions

Rickson C. Mesquita,[1,2,*] Steven S. Schenkel,[1] David L. Minkoff,[1] Xiangping Lu,[3] Christopher G. Favilla,[3] Patrick M. Vora,[1] David R. Busch,[1,4] Malavika Chandra,[1] Joel H. Greenberg,[3] John A. Detre,[3,5] and A. G. Yodh[1]

[1]*Department of Physics & Astronomy, University of Pennsylvania, 3231 Walnut St., Philadelphia, PA 19104, USA*
[2]*Institute of Physics, University of Campinas, 777 Sergio Buarque de Holanda St., Campinas, SP 13083-859, Brazil*
[3]*Department of Neurology, University of Pennsylvania, 3400 Spruce St., Philadelphia, PA 19104, USA*
[4]*Department of Pediatrics, Division of Neurology, Children's Hospital of Philadelphia, 34th St. & Civic Center Blvd., Philadelphia, PA 19104, USA*
[5]*Department of Radiology, University of Pennsylvania, 3400 Spruce St., Philadelphia, PA 19104, USA*
**rickson@ifi.unicamp.br*

Abstract: A pilot study explores relative contributions of extra-cerebral (scalp/skull) versus brain (cerebral) tissues to the blood flow index determined by diffuse correlation spectroscopy (DCS). Microvascular DCS flow measurements were made on the head during baseline and breath-holding/hyperventilation tasks, both with and without pressure. Baseline (resting) data enabled estimation of extra-cerebral flow signals and their pressure dependencies. A simple two-component model was used to derive baseline and activated cerebral blood flow (CBF) signals, and the DCS flow indices were also cross-correlated with concurrent Transcranial Doppler Ultrasound (TCD) blood velocity measurements. The study suggests new pressure-dependent experimental paradigms for elucidation of blood flow contributions from extra-cerebral and cerebral tissues.

OCIS codes: (170.3880) Medical and biological imaging; (170.2655) Functional monitoring and imaging; (170.3660) Light propagation in tissues; (170.6480) Spectroscopy, speckle.

References and links

1. E. I. Dieters, S. H. Hidding, M. Kalisvaart, and E. G. Mik, "Near infrared spectroscopy: an asset to the diagnosis and treatment of traumatic brain injury," Erasmus J. Med. **1**(2), 23–26 (2011).
2. T. Durduran, C. Zhou, B. L. Edlow, G. Yu, R. Choe, M. N. Kim, B. L. Cucchiara, M. E. Putt, Q. Shah, S. E. Kasner, J. H. Greenberg, A. G. Yodh, and J. A. Detre, "Transcranial optical monitoring of cerebrovascular hemodynamics in acute stroke patients," Opt. Express **17**(5), 3884–3902 (2009).
3. H. Obrig and J. Steinbrink, "Non-invasive optical imaging of stroke," Philos. Trans. R. Soc. A **369**(1955), 4470–4494 (2011).
4. S. Muehlschlegel, J. Selb, M. Patel, S. G. Diamond, M. A. Franceschini, A. G. Sorensen, D. A. Boas, and L. H. Schwamm, "Feasibility of NIRS in the neurointensive care unit: a pilot study in stroke using physiological oscillations," Neurocrit. Care **11**(2), 288–295 (2009).
5. C. Kolyva, H. Kingston, I. Tachtsidis, S. Mohanty, S. Mishra, R. Patnaik, R. J. Maude, A. M. Dondorp, and C. E. Elwell, "Oscillations in cerebral haemodynamics in patients with falciparum malaria," Adv. Exp. Med. Biol. **765**, 101–107 (2013).
6. H. Tsunashima, K. Yanagisawa, and M. Iwadate, "Measurement of brain function using near-infrared spectroscopy (NIRS)," in *Neuroimaging – Methods*, P. Bright, ed. (InTech, 2012).
7. D. R. Leff, F. Orihuela-Espina, C. E. Elwell, T. Athanasiou, D. T. Delpy, A. W. Darzi, and G. Z. Yang, "Assessment of the cerebral cortex during motor task behaviours in adults: a systematic review of functional near infrared spectroscopy (fNIRS) studies," Neuroimage **54**(4), 2922–2936 (2011).
8. S. M. Liao, S. L. Ferradal, B. R. White, N. Gregg, T. E. Inder, and J. P. Culver, "High-density diffuse optical tomography of term infant visual cortex in the nursery," J. Biomed. Opt. **17**(8), 081414 (2012).
9. T. Durduran, G. Yu, M. G. Burnett, J. A. Detre, J. H. Greenberg, J. Wang, C. Zhou, and A. G. Yodh, "Diffuse optical measurement of blood flow, blood oxygenation, and metabolism in a human brain during sensorimotor cortex activation," Opt. Lett. **29**(15), 1766–1768 (2004).

#187602 - $15.00 USD Received 22 Mar 2013; revised 13 May 2013; accepted 14 May 2013; published 3 Jun 2013

10. R. C. Mesquita, M. A. Franceschini, and D. A. Boas, "Resting state functional connectivity of the whole head with near-infrared spectroscopy," Biomed. Opt. Express **1**(1), 324–336 (2010).
11. D. A. Boas, L. E. Campbell, and A. G. Yodh, "Scattering and imaging with diffusing temporal field correlations," Phys. Rev. Lett. **75**(9), 1855–1858 (1995).
12. T. Durduran, R. Choe, W. B. Baker, and A. G. Yodh, "Diffuse optics for tissue monitoring and tomography," Rep. Prog. Phys. **73**(7), 076701 (2010).
13. G. Yu, T. Durduran, C. Zhou, R. Cheng, and A. G. Yodh, "Near-infrared diffuse correlation spectroscopy for assessment of tissue blood flow," in *Handbook of Biomedical Optics*, D. A. Boas, C. Pitris, and N. Ramanujam, eds. (CRC Press, 2011).
14. R. C. Mesquita, T. Durduran, G. Yu, E. M. Buckley, M. N. Kim, C. Zhou, R. Choe, U. Sunar, and A. G. Yodh, "Direct measurement of tissue blood flow and metabolism with diffuse optics," Philos. Trans. R. Soc. A **369**(1955), 4390–4406 (2011).
15. R. C. Mesquita, N. Skuli, M. N. Kim, J. Liang, S. S. Schenkel, A. J. Majmundar, M. C. Simon, and A. G. Yodh, "Hemodynamic and metabolic diffuse optical monitoring in a mouse model of hindlimb ischemia," Biomed. Opt. Express **1**(4), 1173–1187 (2010).
16. S. A. Carp, G. P. Dai, D. A. Boas, M. A. Franceschini, and Y. R. Kim, "Validation of diffuse correlation spectroscopy measurements of rodent cerebral blood flow with simultaneous arterial spin labeling MRI; towards MRI-optical continuous cerebral metabolic monitoring," Biomed. Opt. Express **1**(2), 553–565 (2010).
17. R. C. Mesquita, S. W. Han, J. Miller, S. S. Schenkel, A. Pole, T. V. Esipova, S. A. Vinogradov, M. E. Putt, A. G. Yodh, and T. M. Busch, "Tumor blood flow differs between mouse strains: consequences for vasoresponse to photodynamic therapy," PLoS ONE **7**(5), e37322 (2012).
18. J. P. Culver, T. Durduran, D. Furuya, C. Cheung, J. H. Greenberg, and A. G. Yodh, "Diffuse optical tomography of cerebral blood flow, oxygenation, and metabolism in rat during focal ischemia," J. Cereb. Blood Flow Metab. **23**(8), 911–924 (2003).
19. F. Jaillon, J. Li, G. Dietsche, T. Elbert, and T. Gisler, "Activity of the human visual cortex measured non-invasively by diffusing-wave spectroscopy," Opt. Express **15**(11), 6643–6650 (2007).
20. B. L. Edlow, M. N. Kim, T. Durduran, C. Zhou, M. E. Putt, A. G. Yodh, J. H. Greenberg, and J. A. Detre, "The effects of healthy aging on cerebral hemodynamic responses to posture change," Physiol. Meas. **31**(4), 477–495 (2010).
21. G. M. Tellis, R. C. Mesquita, and A. G. Yodh, "Use of diffuse correlation spectroscopy to measure brain blood flow differences during speaking and nonspeaking tasks for fluent speakers and persons who stutter," Persp. Fluency Fluency Disord. **21**(3), 96–106 (2011).
22. E. M. Buckley, N. M. Cook, T. Durduran, M. N. Kim, C. Zhou, R. Choe, G. Yu, S. Schultz, C. M. Sehgal, D. J. Licht, P. H. Arger, M. E. Putt, H. H. Hurt, and A. G. Yodh, "Cerebral hemodynamics in preterm infants during positional intervention measured with diffuse correlation spectroscopy and transcranial Doppler ultrasound," Opt. Express **17**(15), 12571–12581 (2009).
23. N. Roche-Labarbe, A. Fenoglio, A. Aggarwal, M. Dehaes, S. A. Carp, M. A. Franceschini, and P. E. Grant, "Near-infrared spectroscopy assessment of cerebral oxygen metabolism in the developing premature brain," J. Cereb. Blood Flow Metab. **32**(3), 481–488 (2012).
24. L. Gagnon, M. A. Yücel, M. Dehaes, R. J. Cooper, K. L. Perdue, J. Selb, T. J. Huppert, R. D. Hoge, and D. A. Boas, "Quantification of the cortical contribution to the NIRS signal over the motor cortex using concurrent NIRS-fMRI measurements," Neuroimage **59**(4), 3933–3940 (2012).
25. R. B. Saager, N. L. Telleri, and A. J. Berger, "Two-detector Corrected Near Infrared Spectroscopy (C-NIRS) detects hemodynamic activation responses more robustly than single-detector NIRS," Neuroimage **55**(4), 1679–1685 (2011).
26. T. Takahashi, Y. Takikawa, R. Kawagoe, S. Shibuya, T. Iwano, and S. Kitazawa, "Influence of skin blood flow on near-infrared spectroscopy signals measured on the forehead during a verbal fluency task," Neuroimage **57**(3), 991–1002 (2011).
27. R. Saager and A. Berger, "Measurement of layer-like hemodynamic trends in scalp and cortex: implications for physiological baseline suppression in functional near-infrared spectroscopy," J. Biomed. Opt. **13**(3), 034017 (2008).
28. R. B. Saager and A. J. Berger, "Direct characterization and removal of interfering absorption trends in two-layer turbid media," J. Opt. Soc. Am. A **22**(9), 1874–1882 (2005).
29. N. M. Gregg, B. R. White, B. W. Zeff, A. J. Berger, and J. P. Culver, "Brain specificity of diffuse optical imaging: improvements from superficial signal regression and tomography," Front. Neuroenergetics **2**, 14 (2010).
30. C. K. Lee, C. W. Sun, P. L. Lee, H. C. Lee, C. Yang, C. P. Jiang, Y. P. Tong, T. C. Yeh, and J. C. Hsieh, "Study of photon migration with various source-detector separations in near-infrared spectroscopic brain imaging based on three-dimensional Monte Carlo modeling," Opt. Express **13**(21), 8339–8348 (2005).
31. T. Durduran, "Non-invasive measurements of tissue hemodynamics with hybrid diffuse optical methods," Ph.D. dissertation (University of Pennsylvania, Philadelphia, 2004).
32. F. Jaillon, S. E. Skipetrov, J. Li, G. Dietsche, G. Maret, and T. Gisler, "Diffusing-wave spectroscopy from head-like tissue phantoms: influence of a non-scattering layer," Opt. Express **14**(22), 10181–10194 (2006).
33. L. Gagnon, M. Desjardins, J. Jehanne-Lacasse, L. Bherer, and F. Lesage, "Investigation of diffuse correlation spectroscopy in multi-layered media including the human head," Opt. Express **16**(20), 15514–15530 (2008).

#187602 - $15.00 USD Received 22 Mar 2013; revised 13 May 2013; accepted 14 May 2013; published 3 Jun 2013

34. B. Hallacoglu, A. Sassaroli, M. Wysocki, E. Guerrero-Berroa, M. Schnaider Beeri, V. Haroutunian, M. Shaul, I. H. Rosenberg, A. M. Troen, and S. Fantini, "Absolute measurement of cerebral optical coefficients, hemoglobin concentration and oxygen saturation in old and young adults with near-infrared spectroscopy," J. Biomed. Opt. **17**(8), 081406 (2012).
35. E. Ohmae, Y. Ouchi, M. Oda, T. Suzuki, S. Nobesawa, T. Kanno, E. Yoshikawa, M. Futatsubashi, Y. Ueda, H. Okada, and Y. Yamashita, "Cerebral hemodynamics evaluation by near-infrared time-resolved spectroscopy: correlation with simultaneous positron emission tomography measurements," Neuroimage **29**(3), 697–705 (2006).
36. J. Heiskala, V. Kolehmainen, T. Tarvainen, J. P. Kaipio, and S. R. Arridge, "Approximation error method can reduce artifacts due to scalp blood flow in optical brain activation imaging," J. Biomed. Opt. **17**(9), 096012 (2012).
37. E. Kirilina, A. Jelzow, A. Heine, M. Niessing, H. Wabnitz, R. Brühl, B. Ittermann, A. M. Jacobs, and I. Tachtsidis, "The physiological origin of task-evoked systemic artefacts in functional near infrared spectroscopy," Neuroimage **61**(1), 70–81 (2012).
38. S. Godfrey and E. J. M. Campbell, "The control of breath holding," Respir. Physiol. **5**(3), 385–400 (1968).
39. T. J. H. Clark and S. Godfrey, "The effect of CO_2 on ventilation and breath-holding during exercise and while breathing through an added resistance," J. Physiol. **201**(3), 551–566 (1969).
40. N. Stocchetti, A. I. R. Maas, A. Chieregato, and A. A. van der Plas, "Hyperventilation in head injury: a review," Chest **127**(5), 1812–1827 (2005).
41. L. Rangel-Castilla, L. R. Lara, S. Gopinath, P. R. Swank, A. Valadka, and C. Robertson, "Cerebral hemodynamic effects of acute hyperoxia and hyperventilation after severe traumatic brain injury," J. Neurotrauma **27**(10), 1853–1863 (2010).
42. T. Moroz, M. Banaji, M. Tisdall, C. E. Cooper, C. E. Elwell, and I. Tachtsidis, "Development of a model to aid NIRS data interpretation: results from a hypercapnia study in healthy adults," Adv. Exp. Med. Biol. **737**, 293–300 (2012).
43. S. Viola, P. Viola, P. Litterio, M. P. Buongarzone, and L. Fiorelli, "Correlation between the arterial pulse wave of the cerebral microcirculation and CBF during breath holding and hyperventilation in human," Clin. Neurophysiol. **123**(10), 1931–1936 (2012).
44. J. M. Clark, B. E. Skolnick, R. Gelfand, R. E. Farber, M. Stierheim, W. C. Stevens, G. Beck, Jr., and C. J. Lambertsen, "Relationship of ^{133}Xe cerebral blood flow to middle cerebral arterial flow velocity in men at rest," J. Cereb. Blood Flow Metab. **16**(6), 1255–1262 (1996).
45. E. Rostrup, I. Law, F. Pott, K. Ide, and G. M. Knudsen, "Cerebral hemodynamics measured with simultaneous PET and near-infrared spectroscopy in humans," Brain Res. **954**(2), 183–193 (2002).
46. J. J. Chen and G. B. Pike, "Global cerebral oxidative metabolism during hypercapnia and hypocapnia in humans: implications for BOLD fMRI," J. Cereb. Blood Flow Metab. **30**(6), 1094–1099 (2010).
47. D. P. Bulte, K. Drescher, and P. Jezzard, "Comparison of hypercapnia-based calibration techniques for measurement of cerebral oxygen metabolism with MRI," Magn. Reson. Med. **61**(2), 391–398 (2009).
48. G. Settakis, A. Lengyel, C. Molnár, D. Bereczki, L. Csiba, and B. Fülesdi, "Transcranial Doppler study of the cerebral hemodynamic changes during breath-holding and hyperventilation tests," J. Neuroimaging **12**(3), 252–258 (2002).

1. Introduction

In-vivo monitoring of brain physiology is an important target area for application of diffuse optical techniques in the clinic. Specifically, the deep tissue penetration of near-infrared light, coupled with its sensitivity to hemodynamic signatures has led to novel studies in critical care monitoring [1–5] and to exploration of the normal functional responses of specific brain networks [6–10]. The vast majority of this work employs the technique of diffuse optical spectroscopy (DOS), or near-infrared spectroscopy (NIRS); DOS probes local oxy- and deoxy-hemoglobin tissue concentrations and variations thereof. A relatively newer optical technique, diffuse correlation spectroscopy (DCS), uses the temporal fluctuations of diffusing near-infrared light fields to access information about blood flow [11–14] and is currently being explored as a means to probe perfusion in animals [15–18] and humans [2,9,19–23]. Finally, the combination of DOS and DCS has very recently proved attractive as a cutting-edge brain diagnostic, because dual information about blood concentration and blood flow can be used to create indices for cerebral oxygen metabolism [2,9,16,23].

Despite these recent advances in the use of DOS and DCS for monitoring cerebral blood flow (CBF) and hemodynamics, the non-invasive brain measurements necessarily involve placement of light sources and detectors on the surface of the head. Therefore, quantification of the relative contributions of scalp, skull and brain tissues to the optical signals is needed. Furthermore, while significant progress has been made modeling DOS/NIRS data from brain

#187602 - $15.00 USD Received 22 Mar 2013; revised 13 May 2013; accepted 14 May 2013; published 3 Jun 2013

[24–30], few studies have critically examined the contributions of extra-cerebral tissues to the DCS blood flow signal [31–33]. Thus, questions about the extra-cerebral contributions to the DCS signal, the optimal source-detector separation for measurement of cortical blood flow, and the effects of probe remain largely unanswered.

The present study aims to elucidate extra-cerebral contributions to the DCS blood flow signal and to characterize the effects of probe pressure. DCS measurements on the human head were made during baseline (resting) and during ventilation-related tasks that alter CBF. These data were derived both with and without pressure applied to the probe, and a simple model that separates the extra-cerebral (scalp/skull) and brain (cerebral) tissue blood flow responses was employed to understand the results. Pressure dependent measurements during baseline conditions revealed that scalp blood flow is indeed sensitive to applied pressure and enabled us to estimate extra-cerebral and brain blood flow signals at all source-detector separations. Further, the use of high probe pressures permitted reliable assessment of changes in microvascular CBF during two global ventilation tasks: breath-holding and hyperventilation. Lastly, the observed microvascular responses were cross-correlated with concurrent Transcranial Doppler Ultrasound (TCD) measurements of blood velocity in the intracranial arteries. The results clearly demonstrate that probe pressure affects extra-cerebral DCS blood flow signals, and they suggest that pressure-dependent measurement paradigms should be useful as a means to distinguish the blood flow contributions of extra-cerebral tissues from those of cerebral tissues.

2. Materials and methods

2.1 Subjects and experimental protocol

Eight healthy subjects were recruited for this study. Subject age ranged from 21 to 30 years, with mean (standard deviation) of 23.4 (3.7) years. (For technical reasons, however, the measurement with applied probe pressure was not carried out in one subject. Therefore, we report on the results of seven subjects (3 male).) Each subject provided written consent, and all protocols/procedures were approved by the Institutional Review Board at the University of Pennsylvania, where the experiments were conducted.

Briefly, each subject was asked to sit comfortably in a chair. The optical probe was then placed on the subject's scalp directly over the right pre-frontal cortex. Resistive pressure sensors were attached to the outside of fiber-containing probe, sandwiched between said probe and another foam pad that held the system in place. In this way we were able to measure the pressure exerted by external forces on the optical probe, e.g., due to the head strap and the TCD head-frame. The entire configuration was held securely in place by a Velcro strap wrapped around the head. The TCD ultrasound probe was placed over the optical configuration. A schematic of this set-up is shown in Fig. 1(A).

The study was divided into two parts that were carried out sequentially, always in the same order. In the first part, minimal pressure was applied on the probe, and blood flow data were acquired for baseline and the breath-holding/hyperventilation tasks. Herein, we refer to these data as either *zero pressure*, *pressure off*, or *no pressure* measurements. In the second part, pressure was applied to the probe by firmly tightening the Velcro straps (but not causing discomfort to the subject). While this higher pressure was maintained, blood flow data were acquired for baseline and the breath-holding/hyperventilation tasks. Herein, we refer to these latter data as *pressure*, or *pressure on* measurements.

In each part of the protocol (pressure off/on), subjects were first required to relax quietly for 5 minutes (baseline period). After this baseline period, the subjects were asked to hold their breath for 25 s (i.e., in the breath-holding task). This task was repeated three times with 60 s of intercalated rest between trials. Afterwards and lastly, the subjects performed three trials of a hyperventilation task that lasted 30 s; 90 s of rest were intercalated between these trials. The hyperventilation task was performed at 1 Hz, and the frequency was controlled by

#187602 - $15.00 USD Received 22 Mar 2013; revised 13 May 2013; accepted 14 May 2013; published 3 Jun 2013

the experimenter. The whole experiment took approximately 40 min. Figure 1(B) summarizes the timing of all the events in the experiment.

2.2 Pressure calibration

The pressure exerted by the probe on the head was measured using thin, flexible, resistive pressure sensors (Tactilus Free Form by Sensor Products and FlexiForce from Tekscan) coupled to a custom (in-house) stabilized voltage circuit and a DAQ board (National Instruments). Two types of pressure sensors were chosen for the study, because the combination was able to discern the entire range of applied pressures with different sensitivities. The sensor units were tested in our lab, e.g., by applying pressure to them over their full specified range; only sensors that showed no hysteresis effects were chosen for mounting on the optical probe. The pressure sensors were then calibrated using an air bladder from a blood pressure cuff and digital pressure gauge (Omega Engineering). Specifically, we placed the air bladder and pressure probe between two rigid parallel plates, and we recorded the output of the sensors over the full range of pressure levels applied to the head.

2.3 DCS acquisition and data analysis

The DCS instrumentation and techniques have been described in detail in previous publications [2,12,14,21]. Briefly, the DCS measurements were performed with an instrument consisting of two continuous-wave, long coherence-length (i.e., >20 m), 785 nm lasers (CrystaLaser Inc., Reno, NV), and two arrays of four avalanche photodiodes (PerkinElmer, Canada). The detection system fed an eight-channel autocorrelator (Correlator.com, Bridgewater, NJ) that computed the temporal autocorrelation function of the detected light intensity. The integration range was between 200 ns and 30 ms so that the large time interval would be sufficient to cover the large changes induced by pressure. The autocorrelation functions were averaged over 3 s to improve signal-to-noise ratio.

The optical probe was arranged in a row configuration with the source at one end and four detectors placed to have source-detector separations along the surface of ρ = 0.5, 1.5, 2.5, and 3.0 centimeters (Fig. 1(A)). One 600 μm-diameter multimode fiber was employed for delivering light, while the detectors at each position consisted of bundles of four 5 μm-diameter single mode fibers (OZ Optics, Ontario, Canada). Black foam rubber material was used to hold each probe in place and to block extraneous light.

Normalized intensity temporal autocorrelation curves, $g_2(\mathbf{r},t,\tau)$, were obtained for each source-detector pair. These data (curves) were fit to the solution of the photon correlation diffusion equation in the semi-infinite geometry with extrapolated zero boundary conditions [12,14]. Since we will be considering both near-surface and deep tissue contributions to the flow/correlation signals, we briefly provide background theory for these measurements.

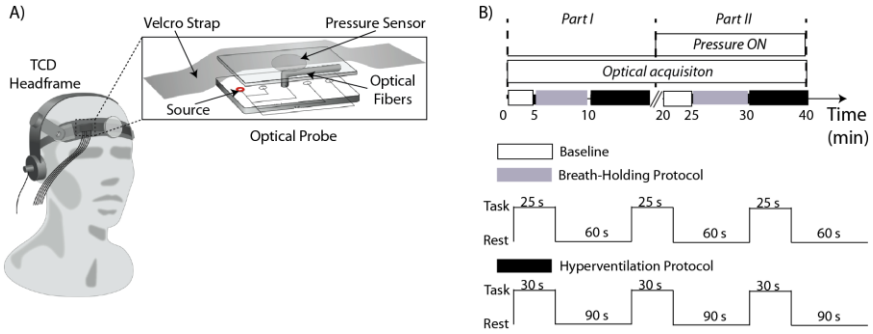

Fig. 1. (A) Experimental setup showing the optical probe schematics. The separations between the sources and detectors were 0.5 cm, 1.5 cm, 2.5 cm, and 3.0 cm. (B) Experiment protocol timeline summarizing the session events.

#187602 - $15.00 USD Received 22 Mar 2013; revised 13 May 2013; accepted 14 May 2013; published 3 Jun 2013

The transport of electric field temporal autocorrelation, $G_1(\mathbf{r},t,\tau)=\langle \mathbf{E}^*(\mathbf{r},t,\tau=0)\,\mathbf{E}(\mathbf{r},t,\tau)\rangle$, through tissue obeys a diffusion equation [11]:

$$\left[\nabla\cdot\left(D(\mathbf{r},t)\nabla\right)-v\mu_a(\mathbf{r},t)-\frac{\alpha}{3}v\mu_s'k_0^2\langle\Delta r^2(t,\tau)\rangle\right]G_1(\mathbf{r},t,\tau)=-vS(\mathbf{r},t,\tau). \quad (1)$$

Here, τ is the correlation time, k_0 is the light wave vector, α represents the fraction of photon scattering events in the tissue from moving scatterers such as red blood cells, and $\langle\Delta r^2(t,\tau)\rangle$ is the mean-square displacement of these moving "particles" in time τ. The brackets denote time averages (for experiments) or ensemble averages (for calculations). The solution of the photon correlation diffusion equation in a homogeneous semi-infinite geometry with extrapolated zero boundary conditions is well known and is given below:

$$G_1(\mathbf{r},t,\tau)=\frac{v}{4\pi D}\left(\frac{e^{-K(\tau)r_1}}{r_1}-\frac{e^{-K(\tau)r_b}}{r_b}\right), \quad (2)$$

where

$$K^2(\tau)=\left(\mu_a(\lambda)+\frac{1}{3}\alpha\mu_s'k_0^2\left\langle\Delta r^2(\tau)\right\rangle\right)/\left(3\mu_s'\right) \quad (3)$$

and r_1 and r_b are given by

$$r_1=\sqrt{(z-l_t)^2+\rho^2} \text{ and } r_b=\sqrt{(z+2z_b+l_t)^2+\rho^2}, \quad (4)$$

respectively. (Note, l_t and z_b depend on the optical parameters and the boundary conditions; their analytical expressions can be found in [12].)

For most DCS experiments in living tissues, the mean-square particle displacement is reasonably well approximated as "effectively" Brownian, i.e., $\langle\Delta r^2(t,\tau)\rangle = 6D_B\tau$, where D_B represents the effective diffusion coefficient of the moving scatterers (which is much larger than the equilibrium Einstein result). Our measured normalized intensity autocorrelation function, $g_2(\mathbf{r},t,\tau) = \langle I^*(\tau=0)I(\tau)\rangle/\langle I(\tau=0)\rangle^2$, is related to the normalized electric field correlation function, $g_1(\mathbf{r},t,\tau) = \langle \mathbf{E}^*(\tau=0)\mathbf{E}(\tau)\rangle/\langle|\mathbf{E}(\tau=0)|^2\rangle$, by the Siegert relation:

$$g_2(\mathbf{r},t,\tau)=1+\beta\left|g_1(\mathbf{r},t,\tau)\right|^2. \quad (5)$$

Here, β is a parameter that depends on the source coherence, detection optics, and other external factors. In order to estimate relative blood flow from the DCS data, we fit all the data points (i.e., with values larger than 1.3) of the measured intensity autocorrelation functions to Eq. (5). The threshold for the fit was chosen in order to decrease the contribution of the photons with short pathlengths and so as not to overweight the tail of the curve. Given the optical properties of the medium, the fits extract the parameter β and a blood flow index, $BFI(t) = \alpha D_B(t)$. For this study, we assumed $\mu_a = 0.1\ cm^{-1}$ and $\mu_s' = 8\ cm^{-1}$ [34] both during baseline and during perturbations. Relative changes in BFI (i.e., rBFI) at time t are defined as $rBFI(t) = BFI(t)/BFI(t_0)$, where t_0 denotes time during the baseline period. Changes in BFI (i.e., ΔBFI) are defined with respect to zero; i.e., $\Delta BFI(\%) = (rBFI-1)\times 100$.

2.4 Physiological model for the autocorrelation function

In order to better understand the contribution of different brain layers to the measured intensity temporal autocorrelation curves as a function of pressure, we developed a simple model for data interpretation. The model attempts to capture physical effects due to applied pressure and due to different source-detector separations. Aspects of this model are similar in

#187602 - $15.00 USD Received 22 Mar 2013; revised 13 May 2013; accepted 14 May 2013; published 3 Jun 2013

spirit to the ideas underlying the differential pathlength method employed in Near-Infrared Spectroscopy (NIRS) with two-layer media [25–28].

The model divides the interrogated tissues into two spatially distinct regions: the near-surface scalp/skull region, which we consider to be "extra-cerebral," and the "brain" region. The model anticipates that probe pressure affects only the extra-cerebral contributions to the DCS signal and, further, that increased probe pressure tends to reduce extra-cerebral blood flow. With respect to source-detector positioning, the model anticipates that signals from small (0.5 cm) source-detector separations will be predominantly (but not necessarily exclusively) extra-cerebral, while signals at large source-detector separations (1.5 cm, 2.5 cm) will contain both extra-cerebral and brain contributions. The model introduces a simple multiplicative source-detector-separation scaling factor to account for the relative importance of brain versus extra-cerebral signal contributions for different source-detector combinations. Other assumptions implicit in this approach (but which can be adjusted) are that the optical properties of the two regions are the same, and that the absolute contributions of the *extra-cerebral* region to the DCS signals are largely independent of our source-detector separation, since light must travel back and forth through approximately the same amount of near-surface tissue for all source-detector separations.

Within this model, the blood flow index (BFI) measured by DCS is given by the sum of the corresponding blood flow indices for the two contributing regions, i.e.,

$$BFI(t,P,\rho) = BF_{ec}(t,P) + \gamma_\rho CBF(t). \tag{6}$$

Here, P represents the pressure exerted by the probe on the scalp, and ρ is the source-detector separation on the tissue surface. BF_{ec} is the blood flow index of the extra-cerebral tissues in the near-surface tissues. CBF is the cerebral blood flow associated with the deeper brain tissues, which is assumed to be independent of pressure. The ρ-dependent factor, γ_ρ, accounts for the increasing cerebral blood flow contribution to the signals at larger source-detector separations; for our range of ρ, we expect this parameter to increase monotonically with ρ, and we expect γ_ρ to be small for ρ = 0.5 cm. In contrast to CBF, the extra-cerebral blood flow contribution, $BF_{ec}(t,P)$, depends on probe pressure, P; we expect $BF_{ec}(t,P)$ to approach zero for large applied probe pressures, and we expect it to decrease monotonically with increasing probe pressure.

This two-region model provides a simple framework that permits better understanding of our DCS flow data. Application of probe pressure provides a mechanism to investigate, account for, and minimize extra-cerebral contributions to the measured signal. For example, measurement of $BFI(t,P,\rho)$ at small ρ and in two pressure conditions (i.e., low/high pressure), permits the absolute contribution of extra-cerebral tissues to the DCS signal to be estimated. This information about the extra-cerebral contributions then enables us to approximate the near-surface (extra-cerebral) flow effects at the other source-detector separations. In a different vein, variation of source-detector separation provides a mechanism to ferret out cerebral contributions to the signal.

Relative measurements of blood flow can also be analyzed within this framework. For example, *rBFI* due to some perturbation (e.g., breath-holding) can be directly related to variation in both the cerebral and extra-cerebral blood flow:

$$rBFI(t) = \frac{BFI(t)}{BFI(t_0)} = 1 + \frac{\Delta BF_{ec}(t,P) + \gamma_\rho \Delta CBF(t)}{BF_{ec}(t_0,P) + \gamma_\rho CBF(t_0)}. \tag{7}$$

In this case, we have explicitly kept the parameters P and ρ in order to remind the reader that these factors can be varied. Here, $\Delta X(\%) = (rX-1) \times 100$, where rX is the relative change in X (i.e., $rX(t) = X(t)/X(t_0)$).

#187602 - $15.00 USD Received 22 Mar 2013; revised 13 May 2013; accepted 14 May 2013; published 3 Jun 2013

From Eq. (7) we see that if the pressure applied on the probe is large enough, then one might reasonably expect $BF_{ec}(t,P)$ and $\Delta BF_{ec}(t,P)$ to be negligible. In this case, rBFI reflects rCBF (ΔCBF) regardless of source-detector separation. Of course, if these factors cannot be neglected, then Eq. (7) and pressure experiments must be used to estimate the relative changes of the cerebral flow signal.

2.5 Transcranial Doppler ultrasound (TCD) measurements

A commercial TCD instrument (Spencer Technologies, Seattle, WA) was utilized to perform concurrent measurements of macrovascular blood velocity. The TCD probe was insonated bilaterally close to the proximal portions of the intracranial arteries, focusing on the Middle Cerebral Artery (MCA). The probe was secured using a Marc 600 Headframe, which provides stable, hands-free vessel insonation throughout the protocol. Signal strength was confirmed prior to initiation of the protocol.

Mean arterial blood velocity (MAv) was collected from both hemispheres, but we used data from the right hemisphere only, since that was the same hemisphere on which the optical probe was positioned. As was the case for the DCS measurements, changes in MAv were measured from zero, relative to a baseline period (i.e., $\Delta MAv(\%)=(MAv(t)/MAv(t_0)-1)\times 100$).

2.6 Statistical analysis

For DCS, the goodness of fit was evaluated for each source-detector separation at each time point, and the decay curves that failed to fit the model were discarded from the analysis (i.e., we rejected curves whose fitting residuals were larger than 75% of the mean residual over the entire time-series). It is worth noting that we did not observe any significant variation of the goodness of fit with applied pressure. For analysis of the absolute BFI, we averaged the entire baseline period before the beginning of the experiment at each condition (with and without pressure). The standard deviation of the mean was chosen as the measure of uncertainty for absolute BFI.

Estimated changes in CBF and MAv were calculated relative to a baseline period for each subject and each pressure condition. For each task trial, baseline was defined as the average of data taken 30 seconds before beginning of the task. Three trials of breath-holding/hyperventilation at the same pressure were averaged, and this average value was assigned as the subject response for that pressure.

In all procedures, data for the whole group were summarized using the median and the interquartile range (IQR). When applicable, data from subgroups of two or three subjects were summarized with mean and standard deviation. Non-parametric Wilcoxon signed rank tests were used to assess statistically significant differences at various time points. All data analysis and statistics were performed with Matlab (MathWorks Inc., Natick, MA).

3. Results

This study explores two types of physiological responses as a function of probe pressure. Measurements during the baseline period, with and without pressure, give information about resting extra-cerebral (scalp/skull) and brain (cerebral) blood flow. These baseline measurements provide an estimate of the size of the baseline scalp/skull blood flow and clearly demonstrate the sensitivity of the extra-cerebral signal to probe pressure. Measurements during the breath-holding and hyperventilation periods, with or without pressure, provide information about ventilation-induced changes in extra-cerebral (scalp/skull) and brain (cerebral) blood flow. Breath-holding is expected to induce an increase in flow, while hyperventilation is expected to induce a decrease in flow. Generally, however, interpretation of the task responses are complicated by the fact that breath-holding and hyperventilation tasks generally induce *global* tissue responses, i.e., responses which might be expected to affect both the scalp/skull and the cerebral hemodynamics. In the *Discussion* section, we critically examine these issues and effects.

#187602 - $15.00 USD Received 22 Mar 2013; revised 13 May 2013; accepted 14 May 2013; published 3 Jun 2013

Seven subjects successfully completed the protocol. However, data from the 3.0 cm source-detector separations were noisy and yielded very large error bars for most subjects. Therefore, we opted to derive conclusions using only those data taken by the first three signal pairs with source-detector separations of 0.5, 1.5 and 2.5 cm.

The optical measurements were obtained over a wide distribution of probe pressures. Across all subjects, the median (IQR) applied pressure was 216 (110, 451) mmHg, and the minimum (maximum) applied pressure across the whole group was 72 (498) mmHg. Herein, the experiments we define as *"pressure off"* employed applied pressures ranging from approximately 20 mmHg to 55 mmHg, i.e., the range of pressures needed to hold the probe in place on the head.

3.1 Influence of pressure during baseline

Figures 2(A)–2(C) show representative examples of measured temporal intensity autocorrelation curves during the *baseline* period for each source-detector separation. Data is shown for *pressure on* and *pressure off* probe configurations. Notice that although the overall temporal dynamics of the curves are similar, the decay rates and derived blood flow index (BFI) differ significantly with and without pressure for the same source-detector separation. Generally, increased applied pressure led to a decrease in absolute BFI.

The phenomenon of decreasing BFI with increasing pressure was larger for the smaller source-detector separations, as can be seen from Fig. 2(D), which plots the estimated baseline rBFI, i.e., $BFI(t_0,P,\rho)/BFI(t_0,P\approx0,\rho)$, for all subjects and pressures. This dependence on the source-detector separation is sensible, since for larger source-detector separations we expect larger contributions from the deep brain tissues to the BFI, i.e., contributions which are independent of pressure. However, since only a few data points were collected, it is difficult to derive quantitative conclusions about the patterns of the BFI drop for the different source-

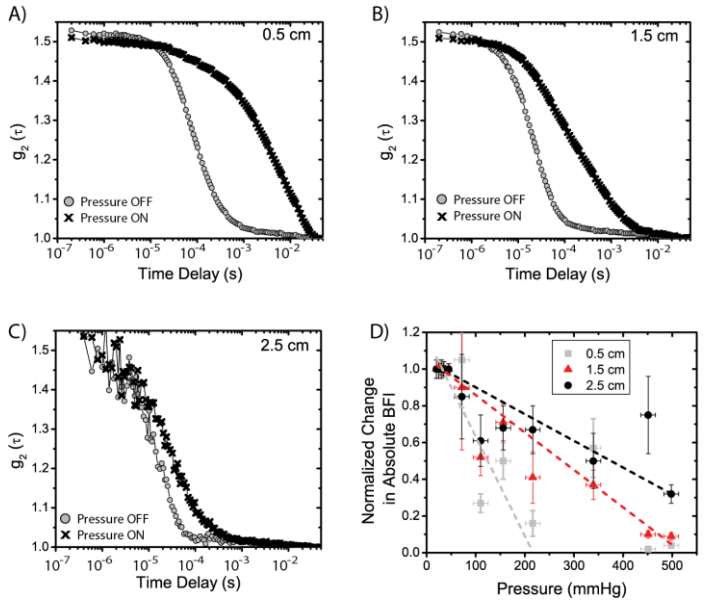

Fig. 2. Representative temporal intensity autocorrelation curves, $g_2(\tau)$, during a baseline time point for a single subject at source-detector separation of (A) 0.5 cm, (B) 1.5 cm, and (C) 2.5 cm. Gray circles (Black crosses) represent baseline measurements without (with) pressure applied to the head by the probe. The fitted decay rate is used to determine the BFI from DCS data. (D) Variation in normalized BFI during baseline as function of applied pressure (see text for normalization definition). Error bars represent the standard deviation of all analyzed baseline frames. The dashed lines are linear fits (see main text).

#187602 - $15.00 USD Received 22 Mar 2013; revised 13 May 2013; accepted 14 May 2013; published 3 Jun 2013

Table 1. Baseline Blood Flow Contributions Estimated by Applying Pressure on the Probe as a Function of Source-Detector Separation[a]

	0.5 cm	1.5 cm	2.5 cm
Baseline extra-cerebral blood flow ($BF_{ec}(t_0,0)$) (cm^2/s)	$2.6(0.9) \times 10^{-9}$	$1.9(0.5) \times 10^{-9}$	$1.4(0.4) \times 10^{-9}$
Baseline brain blood flow ($\gamma_\rho CBF(t_0)$) (cm^2/s)	$0.07(0.06) \times 10^{-9}$	$0.19(0.07) \times 10^{-9}$	$0.9(0.4) \times 10^{-9}$

[a]Considering data from the two subjects with the largest probe pressures applied.

detector separations. As a first approximation, here we report rBFI variations in units of BFI per mmHg using only low-pressure data for the shortest source-detector separation, but we employ linear fits over the full pressure range at the other (larger) source-detector separations. With this approach, absolute BFI was measured to drop by 0.54 (0.03)% per mmHg, 0.20 (0.01)% per mmHg, and 0.15 (0.01)% per mmHg at 0.5, 1.5, and 2.5 cm, respectively. Future research along these lines, but with more comprehensive range of pressures, should permit researchers to discern more complex (e.g., nonlinear) patterns.

We obtain an estimate of the baseline extra-cerebral blood flow, $BF_{ec}(t_0,0)$, using the data from two subjects who experienced the two largest probe pressures (i.e., $P \approx 450$, 498 mmHg). To this end we employ Eq. (6), and set $BF_{ec}(t_0,P) \approx 0$ at the two highest probe pressures, in order to derive an estimate for baseline extra-cerebral blood flow; as an example, for the shortest source-detector separation and the highest pressure, we obtain the following estimate for baseline extra-cerebral blood flow: $BF_{ec}(t_0,0) = [BFI(t_0,P\approx 0,\rho) - BFI(t_0,P\approx 498,\rho)]$. Similar expressions can be derived for other pressures (i.e., other large pressures) and other source-detector separations. For these two subjects, baseline BF_{ec} was found to have a mean (standard deviation) of $2.6(0.9) \times 10^{-9}$ cm^2/s using the 0.5 cm source-detector separation. At the other source-detector separations the measurement signal-to-noise is reduced, because the CBF contributions are relatively more significant and the signal intensity is smaller than at 0.5 cm. Nevertheless, our estimate for baseline extra-cerebral blood flow was similar at all source-detector separations, considering error bars (Table 1).

Using the temporal decay data and $BF_{ec}(t_0,0)$, we can also estimate the brain (cerebral) contribution to the total decay rate with *pressure off*. As it can be seen from Table 1, the contribution of brain is significantly lower than the extra-cerebral contribution with *pressure off*, especially at the shortest source-detector separations.

Further, by assuming that CBF does not change with pressure, one can use Eq. (6) and the measurements to derive the ratio of γ_ρ at different source-detector separations. For example, using the same two subjects above we can estimate the mean (standard deviation) of the ratios of the source-detector-dependent multiplicative factors in Eq. (6), i.e., $\gamma_{0.5}/\gamma_{2.5} = 0.07(0.04)$, $\gamma_{1.5}/\gamma_{2.5} = 0.19(0.07)$.

3.2 Influence of pressure with global perturbations

After quantifying the extra-cerebral signals with and without applied pressure at baseline, we sought to characterize physiologic responses of BF_{ec} and CBF to simple ventilation perturbations measured with and without applied pressure. To this end, the subjects performed two tasks: breath-holding and hyperventilation. These tasks are known to change blood flow *globally*, i.e., in both extra-cerebral tissues and brain tissues, albeit not necessarily by the same amount.

Figures 3(A)–3(B) show time courses of the relative changes in BFI estimated during the breath-holding task for one representative subject, both with and without applied pressure. With *minimal* pressure applied to the probe (i.e., *pressure off* condition), BFI was found to increase across the subject group with median (IQR) variation of 19.3 (8.4, 50)%, 25.9 (7.5, 68)% and 22.5 (17, 55)% at 0.5 cm, 1.5 cm and 2.5 cm, respectively. The MAv from TCD was also obtained and it increased across the group by 26.1 (22, 39)%.

#187602 - $15.00 USD Received 22 Mar 2013; revised 13 May 2013; accepted 14 May 2013; published 3 Jun 2013

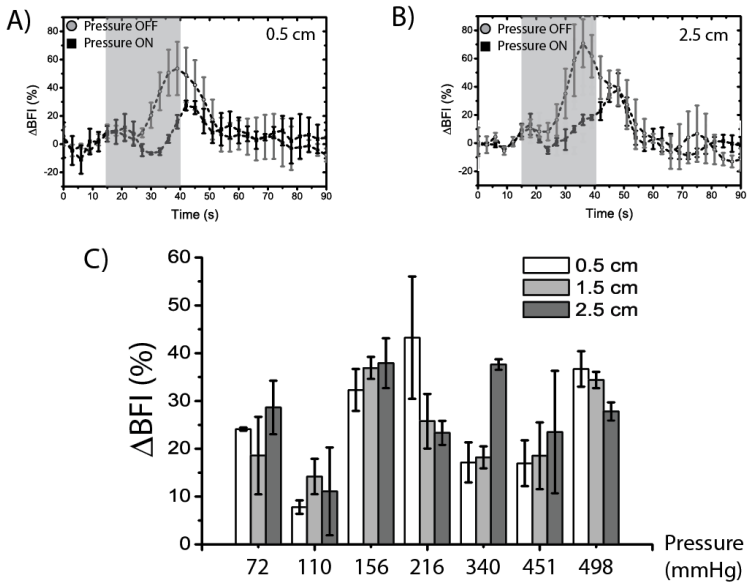

Fig. 3. Representative average CBF response during breath-holding task for a single subject at (A) 0.5 cm and (B) 2.5 cm source-detector separations, both in the absence (gray circles) and in the presence (black squares) of applied pressure on the probe. The shaded area represents the task period. (C) Maximum change in BFI, as function of pressure, during the breath-holding intervention.

Figure 3(C) shows the maximum change from baseline of BFI during breath-holding as a function of applied pressure for each subject. Interestingly, no clear trend was apparent for the behavior of the measured perfusion changes, regardless of the applied pressure. For all subjects under all applied pressures, we found a median (IQR) increase of 24.1 (17, 50)%, 18.6 (18, 37)%, and 28.6 (23, 38)% at 0.5 cm, 1.5 cm and 2.5 cm, respectively. As might be expected, MAv from TCD was not affected by pressure and showed an increase of 25.3 (18, 30)%. Inspection of these data show further that the variance of DCS-measured BFI changes is reduced by increased probe pressure, and that the agreement between DCS-measured and TCD-measured BFI changes is improved at increased probe pressure, i.e., by contrast with the "no pressure" state. Considering only the two subjects at our highest pressures (~500 mmHg), i.e., for which extra-cerebral blood flow might be expected to be very small, we measured a breath-holding induced change in flow of 26.9 (4.4)%, 26.5 (4.1)% and 25.7(7.2) % at 0.5 cm, 1.5 cm and 2.5 cm, respectively. The change in MAv due to breath-holding for these two subjects was 21.9 (2.2)%. As noted above, at these high pressures, we expect the extra-cerebral blood flow signals to be small (see results from Section 3.1 during the baseline period) so that we should predominantly be measuring cerebral response.

Figures 4(A)–4(B) show representative time courses of the relative changes in BFI during the hyperventilation intervention for a single subject. In this case, across the group and at low probe pressure, activated BFI was found to decrease compared to baseline by a median (IQR) of −10.6 (−16.7, −7.7)%, −13.6 (−22.2, −10.4)%, and −25.9 (−31.5, −11.3)% at 0.5 cm, 1.5 cm, and 2.5 cm, respectively. Simultaneous measurements of TCD yielded a median (IQR) decrease of −26.6 (−30.9, −18.8)% due to hyperventilation.

As was the case with breath-holding, increased applied pressure on the probe resulted in decreased variation of the DCS-measured changes for all subjects (Fig. 4(C)). The changes due to hyperventilation with probe pressure were more robust and relatively constant across the range of pressures measured, i.e., when compared to the changes obtained with minimal probe pressure. Overall, we found a median (IQR) decrease of −14.4 (−19.2, −12.8)%, −16.4

#187602 - $15.00 USD Received 22 Mar 2013; revised 13 May 2013; accepted 14 May 2013; published 3 Jun 2013

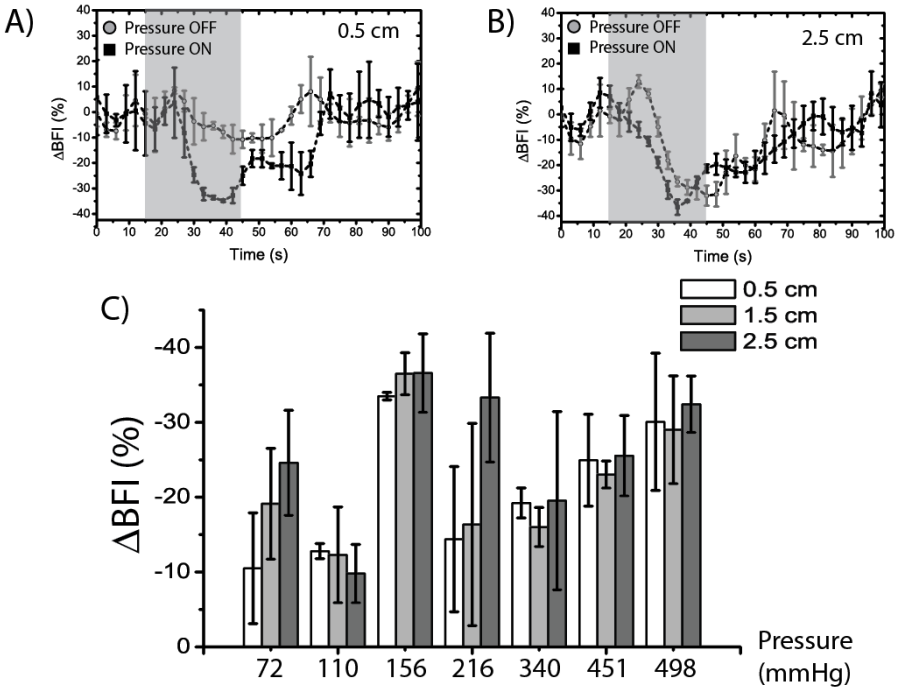

Fig. 4. Representative average CBF response during the hyperventilation task for a single subject at (A) 0.5 cm and (B) 2.5 cm source-detector separations, both in the absence (gray circles) and in the presence (black squares) of applied pressure on the probe. The shaded area represents the task period. (C) Minimum change in BFI, as function of pressure, during the hyperventilation intervention.

(–19.1, –15.5)%, and –25.5 (–33.3, –19.5)% at 0.5 cm, 1.5 cm, and 2.5 cm, respectively. MAv showed a median (IQR) decrease of –28.9 (–36.8, –26.1)% due to hyperventilation, similar to the change found when no pressure was applied.

Again, considering only the two subjects with the highest applied pressures (~500 mmHg), i.e., for which extra-cerebral blood flow might be expected to be very small, the changes measured optically at all source-detector separations were close to those measured by TCD. The BFI change was –27.5 (5.4)%, –26.1 (3.4)% and –29.0 (3.5)% at 0.5, 1.5 and 2.5 cm, respectively. The MAv decrease for these subjects was –31.6 (2.5)%. Table 2 summarizes all the results found for both perturbations under the different pressure protocols.

Table 2. Perfusion Changes Measured During Ventilation Induced Perturbations

	ΔBFI (DCS)			ΔMAv (TCD)
	0.5 cm	1.5 cm	2.5 cm	
Breath-holding				
Pressure off[a]	19.3 (8.4, 50)%	25.9 (7.5, 68)%	22.5 (17, 55)%	26.1 (22, 39)%
Pressure on[a]	24.1 (17, 50)%	18.6 (18, 37)%	28.6 (23, 38)%	25.3 (18, 30)%
Highest pressure[b]	26.9 (4.4)%	26.5 (4.1)%	25.7(7.2) %	21.9 (2.2)%
Hyperventilation				
Pressure off[a]	–10.6 (–17, –7.7)%	–13.6 (–22, –10)%	–25.9 (–32, –11)%	–26.6 (–31, –19)%
Pressure on[a]	–14.4 (–19, –13)%	–16.4 (–19, –16)%	–25.5 (–33, –20)%	–28.9 (–37, –26)%
Highest pressure[b]	–27.5 (5.4)%	–26.1 (3.4)%	–29.0 (3.5)%	–31.6 (2.5)%

[a]Changes reflect the median (inter-quartile range) over all subjects.
[b]Data shown represent the mean (standard deviation) over the two subjects who experience large pressure.

#187602 - $15.00 USD Received 22 Mar 2013; revised 13 May 2013; accepted 14 May 2013; published 3 Jun 2013

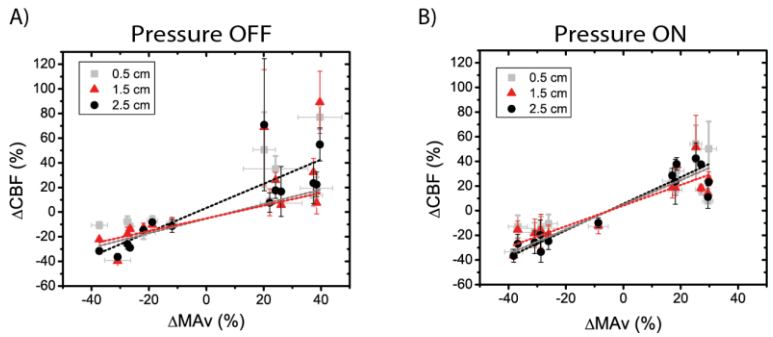

Fig. 5. Scatter plot comparing DCS and TCD measured changes due to both breath-holding and hyperventilation tasks, for source-detector separations of 0.5 cm (blue), 1.5 cm (red) and 2.5 cm (black), respectively, when (A) no pressure was applied on the probe and when (B) pressure was applied on the probe. The error bars represent the standard error over the three different tasks per subject, and the solid lines represent the best linear fit of the data.

3.3 Comparison with TCD

Lastly, we compared microvascular changes in BFI, as measured by DCS, with macrovascular changes in blood velocity, as measured by TCD, during both the breath-holding and the hyperventilation tasks (Fig. 5). The changes in these two independent hemodynamic parameters were significantly correlated, even at small source-detector separations. When minimal probe pressure was applied, the correlation between changes in BFI and changes in MAv yielded R-values of 0.79, 0.82 and 0.86 for DCS source-detector separations of 0.5 cm, 1.5 cm and 2.5 cm, respectively. However, the R-values were measurably larger when pressure was applied to the probe, i.e., 0.97, 0.91 and 0.94 for DCS changes measured at source-detector separations of 0.5 cm, 1.5 cm and 2.5 cm, respectively.

The slope of the DCS-BFI versus MAv correlation plots were estimated to have mean (standard error) of 0.59 (0.03), 0.52 (0.03) and 0.98 (0.07) for separations of 0.5 cm, 1.5 cm and 2.5 cm, respectively, when no pressure was applied; notice that a 1:1 change in MAv and DCS is only indicated at the 2.5 cm separation. Interestingly, when we applied pressure on the probe, the slopes were closer to unity at all source-detector separations, yielding 0.99 (0.01), 0.84 (0.04) and 1.08 (0.05) for separations of 0.5 cm, 1.5 cm and 2.5 cm, respectively. In all cases, the intercept was not statistically different from zero. Table 3 summarizes our findings for the comparison between DCS and TCD.

Table 3. DCS Comparison with TCD Measurements During Perturbation

	R-value			Slope		
	0.5 cm	1.5 cm	2.5 cm	0.5 cm	1.5 cm	2.5 cm
Pressure on	0.79	0.82	0.86	0.59 (0.03)	0.52 (0.03)	0.98 (0.07)
Pressure off	0.97	0.91	0.94	0.99 (0.01)	0.84 (0.04)	1.08 (0.05)

4. Discussion

In this study, the effects of pressure on the DCS blood flow signal were investigated for optical probes placed on the head over intact scalp and skull. Blood flow signals were derived at baseline (resting) and during two ventilatory tasks as a function of applied probe pressure. Our goal was to ascertain the contributions of extra-cerebral and brain (cerebral) tissues to the signal as a function of applied probe pressure and source-detector separation. We also compared the microvascular optical flow data to concurrent measurements of macrovascular blood flow using TCD.

In studies of human brain, optical techniques such as diffuse optical tomography/spectroscopy (DOS/DOT), near infrared spectroscopy (NIRS), and diffuse correlation spectroscopy (DCS), require placement of the sources and detectors on the head

#187602 - $15.00 USD Received 22 Mar 2013; revised 13 May 2013; accepted 14 May 2013; published 3 Jun 2013

over scalp and skull. Thus the detected light must travel significant distance through extra-cerebral tissues, and even though the scalp and skull flow might be expected to be only about 10-15% that of the cortex [35], its contribution to the optical signals can be significant and can lead experimenters to incorrectly assign physiological responses to deeper brain tissues. Here, our focus is on blood flow and, in particular, on the relative extra-cerebral and brain (cerebral) components of the DCS flow signal. We hypothesized that application of pressure to the optical probe (which is transmitted to the tissues in contact with the probe) would alter the extra-cerebral contributions and perhaps minimize them at the highest pressures. In this case, since blood flow in the skull is lower than in scalp and brain, one might anticipate a reduction in scalp flow and a relative increase in the cortical contribution to the measured DCS signal.

To date, a few NIRS (DOS) studies have observed that a significant contribution to measured task-related changes in chromophore concentration are a result of task-related changes in extra-cerebral hemodynamics (i.e., skin/scalp and skull) [24,26,35–37]. One of these studies reported that the NIRS signal (i.e., both extra-cerebral and brain signal) can drop to zero when the pressures applied to the optical probe range from approximately 350 to 1200 mmHg [26]; they attributed this drop to suppression of skin blood flow. Here, we have carried out a related study that focuses on blood flow signals from brain derived by DCS; note, we employed pressures in the lower range of the previous NIRS study [26] in order to preserve subject comfort. Since most of the pressures applied in our study were greater than peak systolic pressure, we expect that pressure effects should prevent inflow to the scalp tissue under the probe and should reduce blood volume in the region. Other techniques currently employed to measure scalp blood flow, such as Laser Doppler Flowmetry, could provide direct evidence to support this assumption. Thus, here, we have presented indirect evidence that the extra-cerebral contributions to the tissue blood flow appear to vanish at the highest pressures. This evidence is consistent with previous findings of NIRS. Clearly future studies are needed to affirm these conclusions; for example, it would be good to independently confirm that pressures under the probe are uniform, to measure the size of extra-cerebral signals from the skull, etc.

Our results obtained during baseline (resting) confirm that applied pressure significantly alters the DCS intensity temporal autocorrelation function, reducing the absolute blood flow index (BFI) estimated from its decay rate. The drop in BFI depends on both the pressure applied and the source-detector separation. Large source-detector separations exhibited smaller pressure/no-pressure decrements and lower BFI signal variance as well. This observation makes intuitive sense. Since deeper tissues contribute relatively more than extra-cerebral tissues to the signal at large source-detector separations, the large source-detector separation data should be affected less by pressure. Our blood flow results during the ventilation tasks are more complex but can also be understood with the aid of a simple model for the DCS signal.

In order to quantitatively analyze the effects of pressure on the DCS signal, we developed a simple physiological model for the measured BFI, aiming to separate and elucidate its two main contributors: cerebral (brain) and extra-cerebral (scalp/skull) tissues. As described more completely in the *Methods* section (e.g., Eq. (6)), the model defines an extra-cerebral blood flow contribution, BF_{ec}, which is due to the near-surface tissues and which depends on probe pressure; the extra-cerebral blood flow contribution should approach zero at the largest probe pressures. The second component of the signal is cerebral blood flow, CBF, which is associated with deeper brain tissue; CBF is assumed to be independent of pressure, and its relative contribution to the DCS signal depends on the source-detector separation factor, γ_ρ, which accounts for the increasing CBF contribution at larger source-detector separations. Therefore, our physiological model distinguishes between two types of contributions in a semi-infinite, homogenous medium from which BFI is estimated. We chose to use the semi-infinite homogeneous medium approximation for DCS analysis in this "first attempt," since most of the DCS data in the literature have been analyzed assuming this approach; clearly, a

#187602 - $15.00 USD Received 22 Mar 2013; revised 13 May 2013; accepted 14 May 2013; published 3 Jun 2013

more complete description would consider at least a two-layer model for the diffusion equation, etc. In this vein, more work is needed in the future to take these ideas to the next level, as well as more bench experiments to validate the layered models. With these caveats, the present model, which assumes two physiological components in a semi-infinite homogeneous medium, appears to be a good first approximation for understanding the effects of pressure on flow in the scalp.

This simple model readily provides insight about the absolute BFI measured during baseline in the limit of large pressures. For example, by considering only those subjects whose highest applied pressure was ~500 mmHg, we were able to estimate the contribution of extra-cerebral tissue to the measured BFI by comparing BF_{ec} with and without applied pressure. Further, the contribution of the CBF signal to the measured BFI *increases* with *increasing* ρ, since γ_ρ at 0.5 cm and 1.5 cm is about 7 (4) % and 19 (7) % of the contribution at 2.5 cm, respectively. These fractional contributions are in rough agreement with analytical predictions based on solutions of the diffusion equation for semi-infinite and homogeneous media; i.e., the analytically computed percentage of photons that travel deeper than 1 cm, and are detected at source-detector separations of 0.5 cm and 1.5 cm, is approximately 5% and 29% of the photons detected at 2.5 cm, respectively. Thus the baseline DCS observations are consistent with extra-cerebral (scalp/skull) signals that are quenched with increasing applied pressure.

On the other hand, the differential changes in BFI observed during breath-holding and hyperventilation with and without applied pressure were not substantially different. Superficially, this observation is somewhat surprising in light of the substantial baseline BFI pressure dependences observed. However, it is again possible to understand these results using the model described in the *Methods* section (e.g., Eq. (7)), along with assumptions based on previous observations about the breath-holding and hyperventilation tasks. The breath-holding task is expected to increase the partial pressure of CO_2 and dilate the cerebral vasculature; as a result an increase in blood flow is anticipated [38,39]. The hyperventilation task is expected to decrease the arterial concentration of CO_2, ultimately inducing a decrease in brain blood flow [40,41]. Importantly, both tasks have been previously suggested to induce a global response [42,43]. By global, we mean that the cerebral and the extra-cerebral (scalp/skull) tissues should both exhibit hemodynamic variations in response to the ventilation tasks, although the magnitude of the flow variation across tissue types might be different. Only scalp/skull signals, however, are sensitive to probe pressure.

In the *pressure off* condition, the BFI was measured to increase by approximately 20-30% due to breath-holding, and it was measured to decrease by approximately −25% due to hyperventilation. Given the estimated values for $BF_{ec}(t_0,0)$ from the baseline studies described above, it appears likely that much of this change reflects scalp contributions associated with the tasks, especially for the smaller source-detector separations. More specifically, given the small contribution of CBF to BFI at 0.5 cm source-detector separation, it is quite reasonable to attribute most of the variation in response to scalp changes when no pressure is applied, i.e., differential flow changes of approximately 19 (8, 50)% and −11 (−17, −8)% are due to breath-holding and hyperventilation, respectively. (Note, these scalp changes exhibit large IQR across all the subjects.)

When pressure was applied to the probe, however, a smaller variance in the response to both tasks is observed across the subject population; this reduced variance is reflected in the smaller IQR. Furthermore, for the two subjects with highest pressure (~500 mmHg), all source-detector data gave almost the same numbers for the relative change in BFI due to hyperventilation task. Although unexpected at first, this effect can be deduced from our simple model (Eq. (7)) in the limit that $\Delta BF_{ec}(t,P)$ and $BF_{ec}(t_0,P)$ approach zero at high pressure. In this case, the differential BFI should reflect only changes due to CBF, independent of the source-detector separation (provided γ_ρ is not zero). Using simple semi-infinite medium diffuse theory, we estimate that approximately 1% of the fluence detected at ρ = 0.5 cm comes from photons that have traveled deeper than 1 cm into the medium (i.e.,

#187602 - $15.00 USD Received 22 Mar 2013; revised 13 May 2013; accepted 14 May 2013; published 3 Jun 2013

roughly the distance between the scalp and the external surface of the cortex). Although very tiny, the sensitivity of the 0.5 cm channel to regions deeper than 1 cm below the scalp need not be zero, and the differential change measured in the high pressure limit should approximate that of the cerebral contribution (albeit near its extremal surface). Therefore, the changes of approximately 26 (7.2)% and −28 (5.4)% for breath-holding and hyperventilation, respectively, should reflect changes due to CBF in all source-detector separations, including 0.5 cm. We note, however, that more studies are needed to better understand the limitations of this approach.

Interestingly, the changes measured by DCS at all source-detector separations are consistent with previous reports of CBF changes due to breath-holding and hyperventilation, measured by techniques such as Xe-CT [44], PET [45], ASL-fMRI [46,47] and TCD [48], and they are in the range of the concurrent MAv reported for these two subjects (i.e., 21% and −32% for breath-holding and hyperventilation, respectively). Across the full subject group, we observe that differential BFI is proportional to differential MAv for all source-detector separations, with improved correlation at the higher probe pressures. We note, however, that DCS and TCD measure different quantities, and that they also measure different parts of the vasculature and vascular pathways. Since the details of the mechanisms underlying blood flow changes in the middle cerebral artery (as measured by TCD, assuming that artery diameter does not change significantly), and in the microvasculature (as measured by DCS), is not known, it remains possible that the change could be similar for the specific interventions. Clearly though, one would expect a tighter correlation between these quantities when the optical signal reflects CBF changes, only. In this paper we are approaching these issues as experimentalists; given the assumptions in the analysis, and the measurement ambiguities with respect to cerebral and extra-cerebral contributions, reporting the observations is the best we can do. Again, more work on these issues is desirable in the future.

In all the cases we fitted the BFI assuming constant tissue absorption and scattering properties. While there is certainly evidence in the literature that tissue absorption can change during these perturbations, we note that the effect of absorption does not depend on the correlation time, τ, and, as a result, modest changes in absorption do not strongly affect the extracted blood flow index (which depends largely on the tau-dependent part of the measured correlation function). In other studies carried out in our laboratory, we have found that absorption changes are at most approximately ± 15-25% of the assumed baseline for both protocols (breath-holding and hyperventilation). Thus, as a check on the consequences of the constant absorption assumption, we investigated the effects of absorption changes of such magnitude to the fitted values of BFI, and we found that a 25% change in absorption led to changes ranging from 5% (ρ = 0.5 cm) to 7.5% (ρ = 2.5 cm) in BFI. More importantly, the estimated contributions to the variation of BFI (which depends on the difference between the pressure off and pressure on conditions), including changes in BFI during the perturbations, were of order 2% (or less) in all cases, which is smaller than the statistical error in our study.

In the future it will be important to explore pressure effects in the context of focal cortical activation (e.g., finger-tapping). We note that the breath-holding and hyperventilation tasks were chosen for the present studies because of their simplicity, and because their effects can be directly measured on subject foreheads (without hair) with good signal-to-noise ratio (SNR). Clearly, the global nature of the expected responses complicates the analysis. Also, future DCS studies under pressure combined with corresponding arterial spin-labeling (ASL) MRI could be helpful to further validate the estimated extra-cerebral components and to derive a more localized information/validation about perfusion in the microvasculature. Per future improvements for the model, Monte Carlo simulations could be employed to correct for the assumption that photon pathlengths through the near-surface tissues are the same for all source-detector separations; we expect these corrections to be relatively small, but their implementation should certainly improve upon the model employed in the present paper.

#187602 - $15.00 USD Received 22 Mar 2013; revised 13 May 2013; accepted 14 May 2013; published 3 Jun 2013

One other technical limitation of the measurement scheme is its relatively low SNR because of the small detection area (i.e., due to the use of single-mode fiber detection for DCS). This problem led to noisy data at our largest source-detector separation (3.0 cm). The SNR can be improved by averaging over more single-mode fibers at each detection site, and studies with more available detectors are on-going in our labs. Data from the 3 cm source-detector separations should provide even more sensitivity to CBF than shown in the present paper.

To summarize, we have explored the relative contributions of blood flow signals from extra-cerebral (scalp/skull) and cerebral (brain) tissues to the DCS temporal intensity autocorrelation function. Measurements were made during baseline and ventilation perturbations that alter CBF, both with and without applied pressure. The measurements during baseline (resting) conditions under the high and low pressure conditions enabled us to estimate extra-cerebral flow signals and their pressure dependencies; these measurements were then used within the context of a simple tissue model to estimate baseline CBF versus extra-cerebral signals as a function of source-detector separation. Importantly, the baseline results suggested that the use of high (but still comfortable) probe pressures permits reliable assessment of activated CBF changes, largely independent of source-detector separation. This hypothesis was verified by DCS measurements during two global functional tasks, breath-holding and hyperventilation, which were also cross-correlated with concurrent TCD measurements. The results show that probe pressure affects extra-cerebral DCS signals, and that measurement paradigms that employ pressure can elucidate the blood flow contributions from extra-cerebral and brain tissues. Our initial findings also suggest the need for pressure studies with local cortical activation, rather than global CBF modulation. Such studies are underway in our labs. Future optical probes for monitoring brain physiology may incorporate features to modulate probe pressure to increase the reliability and specificity of the measurements.

Acknowledgments

We are grateful for useful discussions with Turgut Durduran and Regine Choe. This work was supported by the National Institutes of Health (NIH) through R01-NS060653 (AGY), K24-NS058386 (JAD), and P41-EB015893 (AGY and JAD) and by the São Paulo Research Foundation (FAPESP) through 2012/02500-8 (RCM).

#187602 - $15.00 USD Received 22 Mar 2013; revised 13 May 2013; accepted 14 May 2013; published 3 Jun 2013